Momentum Budget of the East Antarctic Atmospheric Boundary Layer: Results of a Regional Climate Model

M. R. VAN DEN BROEKE

Institute for Marine and Atmospheric Research, Utrecht University, Utrecht, Netherlands

N. P. M. VAN LIPZIG AND E. VAN MEIJGAARD

Royal Netherlands Meteorological Institute, de Bilt, Netherlands

(Manuscript received 15 May 2001, in final form 19 April 2002)

ABSTRACT

Output of a regional atmospheric climate model is used to quantify the average January and July momentum budget of the atmospheric boundary layer (ABL) over the East Antarctic ice sheet and the surrounding oceans. Results are binned in nine elevation intervals over the ice sheet and six distance intervals over the ocean. In January, when surface cooling is weak, the large-scale pressure gradient force dominates the ABL momentum budget. In July, under conditions of strong surface cooling, a shallow katabatic jet develops over the gentle slopes of the interior ice sheet and a strong, deep jet over the steep coastal slopes. In the coastal regions the ABL thickens considerably, caused by the piling up of cold air over the adjacent sea ice and ice shelves. This represents the main opposing force for the katabatic winds. Horizontal and vertical advection are generally small. In the cross-slope direction the momentum budget represents a simple balance between surface drag and Coriolis turning. Intraseasonal variability of the large-scale wind field in the ABL can be explained in terms of the strength of the polar vortex, the background baroclinicity, and the topography of the ice sheet. Subsidence is found over the interior ice sheet and rising motion in the coastal zone, reflecting the acceleration and deceleration of the katabatic circulation. However, vertical velocities are generally small, because the downslope mass flux in the ABL is confined to a shallow layer below the wind speed maximum.

1. Introduction

East Antarctica is covered by the largest ice sheet on earth; it has a maximum elevation over 4000 m and a volume equivalent to a global sea level rise exceeding 60 m. The surface of the ice sheet consists of dry snow without the occurrence of melt, except at some areas near sea level. About half of the ice sheet is fringed by 100–1000-m-thick floating ice shelves, and for most of the year sea ice covers the surrounding oceans (Fig. 1).

Two closely coupled meteorological phenomena characterize the East Antarctic atmospheric boundary layer (ABL): a quasi-permanent surface-based temperature inversion (Connolley 1996) and persistent katabatic winds (Parish and Bromwich 1987). The temperature inversion is indirectly caused by the surface radiation deficit: while dry snow absorbs only 15%–20% of the incoming shortwave radiation, it emits longwave radiation nearly as a blackbody. During winter, in the absence of solar radiation, the surface becomes colder than the free atmosphere by as much as 15–30 K and extracts heat from the overlying air through turbulent exchange of sensible heat. Note that from a dynamical point of view, a ''temperature inversion'' is not necessary for negative buoyancy effects to become important in the momentum budget. We prefer the use of ''ABL potential temperature perturbation'' to indicate the difference between ABL and free atmospheric potential temperature. According to this definition, the katabatic or buoyancy forcing is zero outside the ABL. In the case of katabatic flow, the potential temperature perturbation in the ABL is always negative.[1]

Katabatic winds represent the movement of negatively buoyant air over a sloping surface. The magnitude of the katabatic force depends linearly on the temperature perturbation of the air multiplied by the magnitude of the surface slope; that is why the strongest katabatic

Corresponding author address: Dr. Michiel R. van den Broeke, Institute for Marine and Atmospheric Research (IMAU), Utrecht University, P.O. Box 80 005, 3508 TA Utrecht, Netherlands.
E-mail: broeke@phys.uu.nl

[1] In the stable ABL, it is sometimes referred to as the ''potential temperature deficit.''

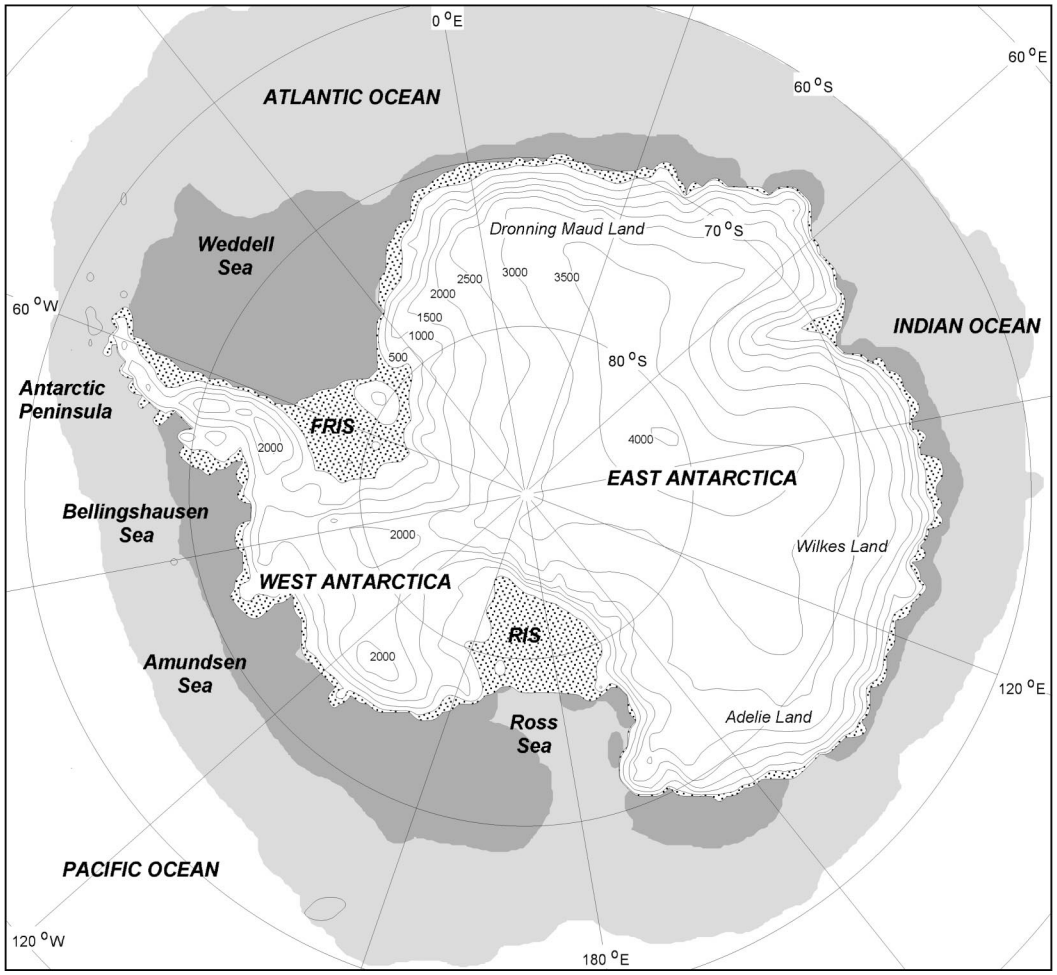

FIG. 1. Model domain and some topographical features of Antarctica. Stippled areas: approximate ice shelf boundaries. Light shaded: average Jul sea ice extent (1980–93). Dark shaded: average Jan sea ice extent (1980–93). Surface elevation (m ASL) is contoured every 500 m. RIS: Ross Ice Shelf; FRIS: Filchner–Ronne Ice Shelf.

winds are found over the steeply sloping ice sheet margins; over the interior ice sheet, winds are considerably weaker (Fig. 2). When the forcing timescale is sufficiently large, as is the case in the Antarctic polar night, the Coriolis effect will deflect the katabatic winds to the left of the topographic fall line. Surface drag maintains a downslope component in a shallow layer below the wind speed maximum. The katabatic force is greatest at the surface, where the temperature perturbation is largest. In combination with surface drag this creates a low level wind speed maximum that is characteristic of katabatic flow. Because the ice sheet topography determines the direction of the forcing, a second characteristic of katabatic flow is its high directional constancy DC, defined as the ratio of the mean to vector mean wind speed (with components u and v):

$$\mathrm{DC} = \frac{(\overline{u}^2 + \overline{v}^2)^{1/2}}{\overline{(u^2 + v^2)^{1/2}}}. \qquad (1)$$

Antarctic katabatic winds rival the trade winds as being the most directionally constant winds on earth, both having a directional constancy exceeding 0.9.

Many observational and modeling studies have been devoted to Antarctic katabatic winds. Observations from manned and automatic weather stations (Wendler et al. 1993; Allison et al. 1993) show that even over the interior ice sheet the large-scale winds are important. Bromwich and Liu (1996) observed at Siple Coast (east coast of the Ross Ice Shelf) that air masses originating from West Antarctica flowed over colder katabatic air originating from the East Antarctic plateau. Parish and Bromwich (1987) noted that channeling of air due to valley-shaped topography can locally enhance katabatic wind speeds. This is particularly true for coastal Adélie Land where the strongest winds on earth are observed; the annual mean wind speed at Cape Denison was 19.4 m s^{-1} in 1912–13 (Schwerdtfeger 1970). Weller (1969) noted that katabatic winds unexpectedly decreased near the coast, associated with an opposing pressure gradient force possibly also responsible for the occurrence of

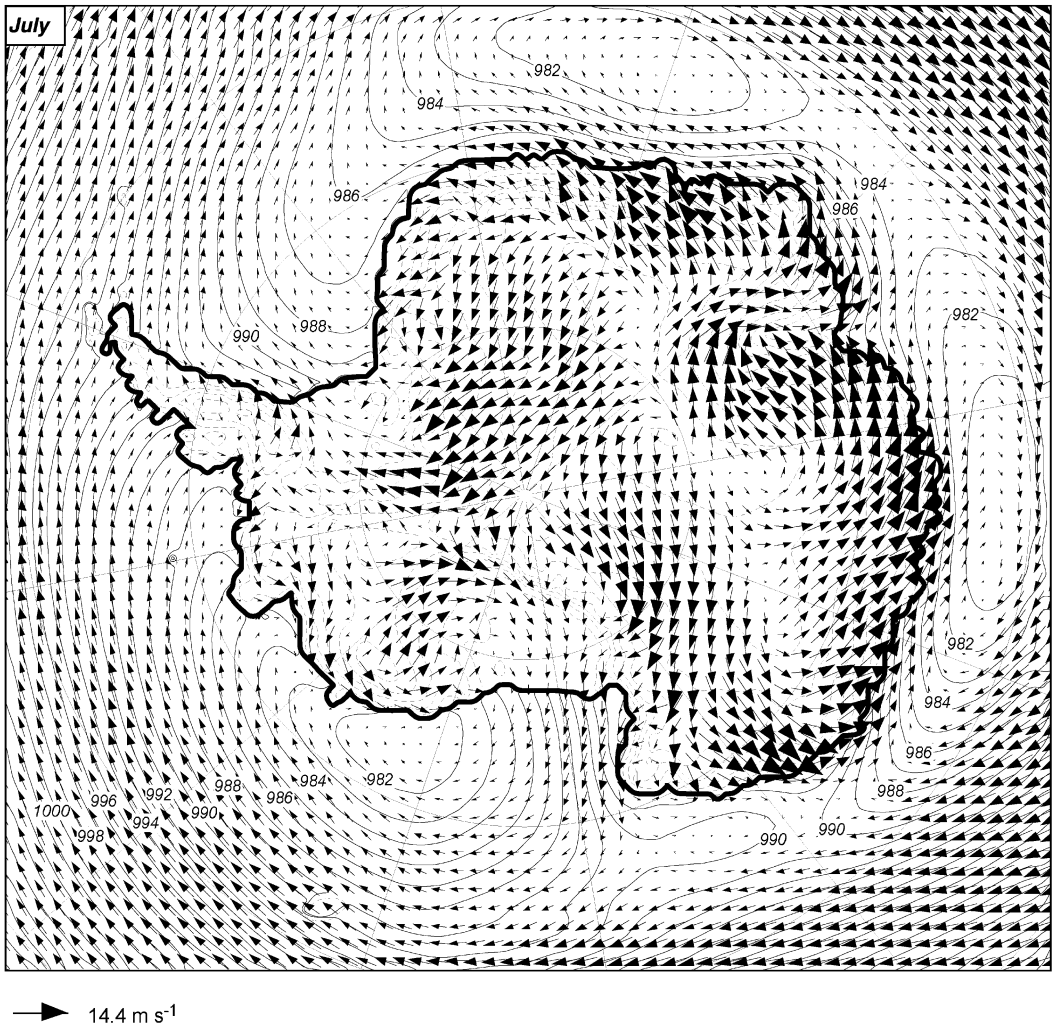

FIG. 2. Average Jul wind vector and sea level pressure from RACMO/ANT1 data (1980–93). Dashed contour lines over the continent represent 500-m elevation intervals, solid labeled contour lines over the sea denote sea level pressure.

hydraulic jumps (Pettré and André 1991). Kodama et al. (1989) observed that near-surface winds in coastal Adélie Land retain their high directional constancy in summer, in spite of the weak or absent temperature perturbation at solar noon. They showed that the large-scale temperature and wind fields created ABL winds with a vertical structure very similar to that of the wintertime katabatic winds.

To explain these observations, a wide range of numerical models of Antarctic katabatic winds has been used. High-resolution models (typically 10–20 km, 2D or 3D) are usually run for a limited domain and period (Parish and Waight 1987; Gallée and Schayes 1992; Bromwich and Du 1994; Gallée et al. 1996; Denby 1999), while continental-scale simulations with regional models usually cover short periods with idealized or absent large-scale circulation (e.g., Hines et al. 1995). General circulation models perform well over Antarctica nowadays (Genthon and Braun 1995; van den Broeke et al. 1997), but there are occasional problems with the representation of the surface (snow versus ice shelves versus sea ice) and the resolution is seldom better than 100–150 km in the horizontal.

A question that only recently has received attention (Parish and Cassano 2001) is how the large-scale pressure gradient force and the pressure gradient force due to ABL inhomogeneites (thermal wind effects) modify the katabatic winds in the East Antarctic ABL. In this paper we use the regional atmospheric climate model over Antarctica, version 1 (RACMO/ANT1; van Lipzig 1999) output to quantify the terms in the ABL momentum balance over Antarctica. This model provides a favorable mix of reasonably high resolution (approximately 55 km $\times$ 55 km), a large domain (122 $\times$ 130 grid points cover entire Antarctica and the surrounding oceans), a 14-yr-long integration period (1980–93), and

realistic boundary conditions. Moreover, the physics package has been especially improved to simulate Antarctic conditions.

In the next section we briefly discuss the model, in section 3 we present the momentum balance for the sloping, stable ABL and how it was calculated from the model output. Section 4 describes the East Antarctic large-scale circulation and temperature fields; sections 5 and 6 discuss the vertical and horizontal distribution of the ABL momentum balance, respectively.

2. Model description

The regional climate model RACMO/ANT1 is based on the ECHAM4 model. The model domain of 122 × 130 gridpoints covers the entirety of Antarctica and part of the surrounding oceans (Fig. 1). At the lateral boundaries, RACMO is forced by 1980–93 European Centre for Medium-Range Weather Forecasts (ECMWF) reanalysis (ERA15) data. Horizontal resolution is approximately 55 km, which enables a reasonably accurate representation of the steep coastal ice slopes and the ice shelves fringing the coast. In the vertical, 20 hybrid levels are used. An additional layer at approximately 7 m above the surface was included to better capture the strong temperature and wind speed gradients near the surface. Several other improvements were made with regard to the physical representation of the snow surface:

- ice shelves were defined as deep snow cover, and no longer partly as sea ice;
- subgrid orographic roughness length was maximized at 3 m;
- albedo was set to a constant value of 0.8;
- heat capacity ($0.804\ 10^6$ J m^{-3} K^{-1}) and diffusivity ($6.06\ 10^{-7}$ m^2 s^{-1}) was for snow, not ice;
- deep snow temperature initialization uses the first two harmonics of the annual temperature signal instead of a cosine function (van Lipzig 1999).

RACMO/ANT1 is a hydrostatic model. The assumption of hydrostatic balance is acceptable in katabatic flows as long as the horizontal length scales dominate the vertical ones (Mahrt 1982), as is usually the case in East Antarctica. Possible exceptions are nocturnal slope flows that develop in the Antarctic summer over local, sub kilometer-steep topography (van den Broeke and Bintanja 1995). Not included in the model are processes related to drifting snow.

In general, the performance RACMO/ANT1 is a great improvement over earlier models (van Lipzig et al. 1998, 1999). In a detailed comparison with station data, van Lipzig (1999) showed that annual mean temperature, wind speed, and directional constancy are generally simulated with rmse's of 1.5 K, 2 m s^{-1}, and 0.12. However, some problems remain. The surface roughness z_0 is composed of a basic value over snow (set to 1 mm) to which is added a contribution from subgrid topographical variance, maximized at 3 m (see above). The latter parameterization leads to overestimated z_0 and underestimated near-surface winds in regions of rough topography (e.g., the Transantarctic Mountains) and, because roughness lengths for heat and moisture z_h and z_q are set equal to z_0, overestimated turbulent exchange of heat and moisture. We have therefore excluded from the present analysis all model gridpoints with $z_0 > 1$ mm. This comprises about 5% of all East Antarctic grid points.

3. Down- and cross-slope momentum budget

We define the positive x axis in the cross-slope direction and the y axis in the downslope direction (Fig. 3); this is done to facilitate comparison with the conditions away from the ice sheet, where the slope direction is undefined and where the usual west–east (x) and south–north (y) coordinate system is adopted. The approximate equation for mean downslope (V) flow on an inclined surface of constant slope α with coordinates (x, y, z) orthogonal to the surface (positive y directed down the slope, positive x directed to the right), can be written as

$$\frac{\partial V}{\partial t} = \underbrace{-U\frac{\partial V}{\partial x}}_{\mathrm{ADVH}_d} \underbrace{- V\frac{\partial V}{\partial y} - W\frac{\partial V}{\partial z}}_{\mathrm{ADVV}_d} + \underbrace{\frac{g}{\Theta_0}\frac{\partial \hat{\Theta} h}{\partial y}}_{\mathrm{THW}_d}$$

$$\underbrace{- fU}_{\mathrm{COR}_d} \underbrace{- fU_{\mathrm{LSC}}}_{\mathrm{LSC}_d} \underbrace{- \frac{\partial \overline{vw}}{\partial z}}_{\mathrm{FDIV}_d} + \underbrace{\frac{g}{\Theta_0}\Delta_\Theta \sin\alpha}_{\mathrm{KAT}}$$

$$\Delta_\Theta = \Theta - \Theta_0$$

$$\hat{\Theta} = \frac{1}{h}\int_z^{h_s+h} \Delta_\Theta(z'')\, dz'', \qquad (2)$$

where the subscript d indicates downslope accelerations, the subscript LSC the large-scale wind components (assumed to be geostrophic), and the subscript 0 background conditions; Δ_Θ is the temperature perturbation of the ABL air relative to Θ_0; $\hat{\Theta}h$ is the vertically integrated temperature perturbation between z and the height of the ABL top $h_s + h$; and (u, v, w) are the components of turbulent velocity fluctuations. KAT is the katabatic pressure gradient force or the horizontal component of the negative buoyancy resulting from a negative temperature perturbation over sloping terrain; LSC represents the large-scale pressure gradient force that drives motion in the ABL over flat terrain; THW represents the thermal wind effects owing to changing temperature perturbation and/or ABL depth, this term drives sea breeze and snow breeze circulations in the ABL over flat terrain. Coriolis deflection of the flow (COR) and vertical divergence of the turbulent momentum flux (FDIV) can be regarded as *passive* forces; that is, they come into play only once motion has been initiated. Horizontal (ADVH) and vertical advection of

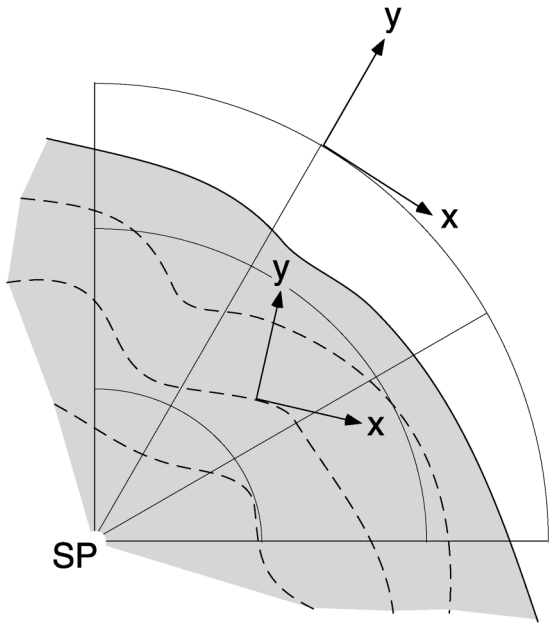

FIG. 3. Orientation of down- and/or cross-slope coordinates over the ice sheet (stippled lines are schematic height contours) and ordinary S–N and W–E coordinates over the ocean (where slope direction is undefined).

momentum (ADVV) are usually small on spatial scales exceeding several tens of kilometers (Kikuchi and Ageta 1989). Special attention is given in this paper to the relative importance of the ''active'' terms in the downslope momentum budget, KAT, LSC_d, and THW_d.

To calculate the magnitude of the terms in the momentum budget, we have to define a background potential temperature Θ_0. In the free troposphere, we assume a linear lapse rate $\gamma_\Theta = \partial\Theta_0/\partial z$ that is constant with height:

$$\Theta_0(z) = \Theta_0(0) + \gamma_\Theta z. \tag{3}$$

Then, $\Theta_0(z)$ in the ABL is obtained by downward extrapolation towards the surface of the monthly mean profiles. To calculate the large-scale pressure gradient force LSC in the ABL we assume that the large-scale wind field (U_{LSC}, V_{LSC}) is in thermal wind balance with Θ_0:

$$\frac{\partial U_{LSC}}{\partial \ln p} = +\frac{R_d}{f}\left(\frac{p}{p_0}\right)^{R_d/c_p}\frac{\partial\Theta_0}{\partial y}$$

$$\frac{\partial V_{LSC}}{\partial \ln p} = -\frac{R_d}{f}\left(\frac{p}{p_0}\right)^{R_d/c_p}\frac{\partial\Theta_0}{\partial x}. \tag{4}$$

The values of (U_{LSC}, V_{LSC}) in the ABL are found using (4) and starting off above the ABL, where we assume the wind to be in geostrophic balance. The term describing the divergence of momentum flux (FDIV) is calculated as a residual, and absorbs model horizontal diffusion and gravity wave drag. If the sum of the other terms is quantitatively correct, FDIV must change sign at the height of the katabatic wind speed maximum; this was the case for all bins.

In the following we present results only from East Antarctica, between longitudes 30°W and 180°. In this sector, katabatic winds are better developed and more horizontally homogeneous than in West Antarctica and the Antarctic Peninsula (Fig. 2). Averages (1980–93) for January (summer) and July (winter) were calculated and, for ease of presentation, subsequently binned in nine surface elevation intervals over the ice sheet and six distance intervals over the ocean. Information on the bins can be found in Table 1.

TABLE 1. Some statistics of the 15 bins. Only points were used between 30°W and 180° longitude and with z_0 = 1 mm over the ice sheet. DTC is distance to coast expressed as position along the *y* axis (negative over the ice sheet).

Bin number	Bin characteristic	Bin name	Area (% of total)	Average elevation (m asl)	Average DTC (km)	Average slope (m km^{-1})
1	>3750 m ASL	High interior	1.1	3858	−1299	1.3
2	3250–3750 m ASL	Middle interior	8.2	3492	−994	1.5
3	2750–3250 m ASL	Low interior	10.2	3011	−849	1.9
4	2250–2750 m ASL	High escarpment	8.3	2514	−588	2.3
5	1750–2250 m ASL	Middle escarpment	3.7	2037	−378	4.0
6	1250–1750 m ASL	Low escarpment	2.0	1531	−224	6.3
7	750–1250 m ASL	High coastal	1.4	1009	−125	9.6
8	150–750 m ASL	Middle coastal	1.5	476	−59	11.2
9	0–150 m ASL	Low coastal	2.8	84	0	2.6
10	0–200 km	Coastal sea	8.0	0	134	0.0
11	200–400 km		9.7	0	302	0.0
12	400–600 km		11.0	0	500	0.0
13	600–800 km		11.0	0	702	0.0
14	800–1000 km		10.9	0	897	0.0
15	1000–1200 km		10.2	0	1098	0.0

4. Large-scale setting: Background potential temperature and zonal wind

In this section we discuss the distribution of background potential temperature and large-scale wind over East Antarctica and the surrounding oceans (Fig. 4). In July (Fig. 4b), the potential temperature near the surface of the interior ice sheet closely follows the 272-K isentropic surface. Moving toward the ocean, the background potential temperature in the ABL slightly increases in the 750–250-km inland distance interval, in response to subsidence induced by the accelerating katabatic winds (see section 6d). Below 1200 m above sea level (ASL), Θ_0 decreases rapidly along the ice sheet surface, when cold and still air over the ice shelves and sea ice is encountered. This represents a region where the meridional temperature gradients are small, resulting in a weak increase or even slight decrease of the large-scale zonal wind with height.

Large-scale disturbances seldom penetrate the 3–4-km-high interior ice sheet, but rather move along the coast. As a result, a climatological circumpolar pressure trough (CPT; Fig. 2) is present just north of the Antarctic continent. In the vicinity of the CPT, three dominant circulation patterns can be discerned:

- Strong and directionally constant large-scale westerlies in the upper troposphere and the winter stratosphere (polar vortex). In midlatitudes, these westerlies prevail also at the surface.
- South of the CPT we find the circumpolar easterlies.
- The katabatic circulation over the ice sheet.

The July upper-air westerlies (representative of the strength of the polar vortex; Fig. 4b) decrease rapidly towards the ice sheet interior. The atmosphere over coastal East Antarctica is highly baroclinic, and the westerlies turn into easterlies at some height above the ice sheet surface. The easterly large-scale wind in the ABL reaches a maximum of about 6 m s^{-1} at 600–700 km inland. Closer to the coast, where upper air westerlies are relatively strong and the thermal wind weaker, easterly large-scale winds in the ABL are also weaker and do not exceed 2–3 m s^{-1}. Note the large-scale wind is easterly everywhere in the ice sheet ABL; that is, LSC_d acts in the same direction as KAT.

In January (Fig. 4a), upper air geostrophic westerlies are weaker, but so is the thermal wind. The net result is that large-scale easterly winds in the ABL over the ice sheet interior are comparable to those in July. In the coastal region, in the absence of a strong westerly jet in the free troposphere, easterly large-scale winds in the ABL are even significantly stronger than in July. This explains the high directional constancy of summertime ABL winds as observed by Kodama et al. (1989).

5. Momentum budget of the East Antarctic ABL: Vertical distribution

The cross-slope momentum balance is a simple balance between $FDIV_c$ and COR_c. Therefore we present only the downslope momentum balance in the following. Figures 5–8 show average vertical profiles of (a) potential temperature, (b) wind components, and (c) downslope momentum budget for January and July for two surface elevation bins:

- middle interior: 3250–3750 m ASL;
- low escarpment: 1250–1750 m ASL.

a. January

In January, the surface potential temperature deficit in the middle interior is typically 6 K (Fig. 5a); the resulting katabatic force is sufficiently large to drive stronger-than-large-scale winds up to 1500 m above the surface (Fig. 5b). LSC_d dominates the downslope momentum budget (Fig. 5c), in spite of weak large-scale winds of 2–4 m s^{-1}. Horizontal and vertical advection and thermal wind effects are small. In the low escarpment, relatively warm, moist air masses increase the downwelling longwave radiation compared to the interior, which limits the surface potential temperature deficit to approximately 5 K (Fig. 6a) and even less than that in the coastal bin (not shown). These low values are in agreement with observations from the Antarctic coastal station Mawson (Streten 1990). The large-scale easterlies in the ABL are relatively strong, >5 m s^{-1} near the surface (Fig. 6b). KAT nevertheless exceeds LSC_d near the surface, owing to the steep surface slope (Fig. 6c). Again, advection is small throughout the ABL, but THW_d is now a significant positive forcing. This results from a decreasing vertically integrated potential temperature deficit coastward (not shown).

b. July

In the polar night, latent heat exchange and subsurface heat transport are small at the surface of the interior ice sheet (van den Broeke 1997), and the surface energy budget is determined by the net longwave radiation (sink) and the turbulent flux of sensible heat (source). When ABL winds are moreover weak, the stable stratification of the surface layer inhibits turbulent exchange and the net longwave radiation becomes the sole term of importance. The emissivity of snow (approximately 0.98) being far greater than that of the clear, dry atmosphere (King 1996), the surface temperature must be considerably lower than the air temperature to set up a longwave balance at the surface. This explains the very large negative surface temperature perturbation in the middle interior of more than 30 K (Fig. 7a). These values are confirmed by observations from interior stations such as Vostok and South Pole (Connolley 1996). In the absence of strong turbulence the cold layer remains shallow, and only in the lowest 100 m of the ABL does KAT dominate the momentum balance (Fig. 7c). Note again the considerable contribution of the large scale wind to the total wind speed. Besides a slight opposing

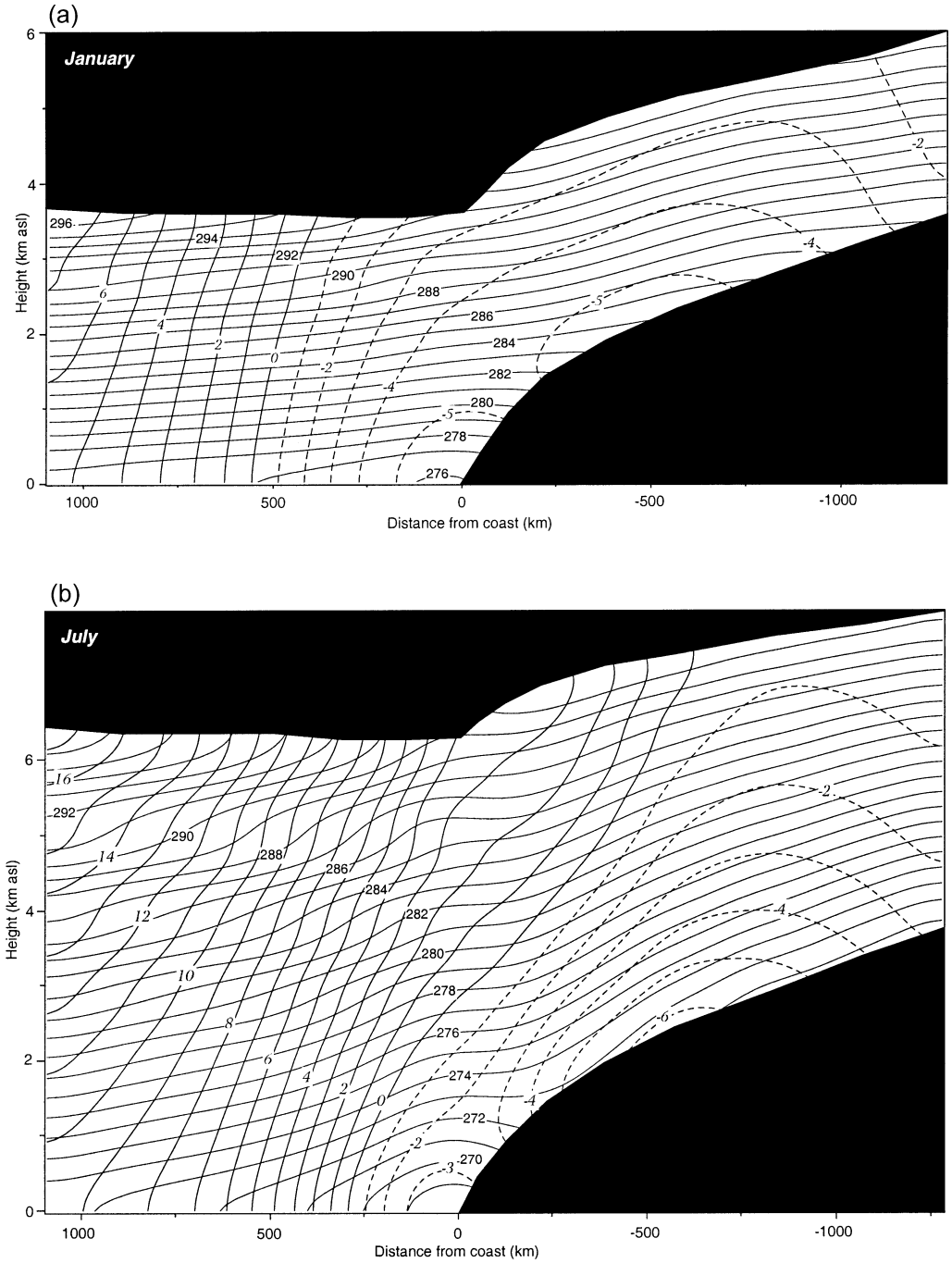

FIG. 4. Average cross sections of background potential temperature Θ_0 (K) (plain contour labels) and large-scale wind (cross-slope component over the ice sheet; W–E component over the ocean; italic contour labels) for (a) Jan and (b) Jul. Only ABL and that part of the troposphere that was used in the extrapolation procedure (see text) are shown.

THW_d and surface drag $FDIV_d$ in a shallow layer near the surface, only turning of the wind by the Coriolis force balances the downslope forcing.

In the lower escarpment the surface potential temperature perturbation is still about 20 K (Fig. 8a). The large-scale zonal wind speed is relatively large, up to 6 m s^{-1} at the surface (Fig. 6b). Note that already at 2.5 km above the surface, large-scale winds have turned to westerlies. This is the region of strongest baroclinicity in East Antarctica (van den Broeke and van Lipzig 2002, manuscript submitted to *Mon. Wea. Rev.*), where the atmospheric layer with large-scale easterlies is thinnest

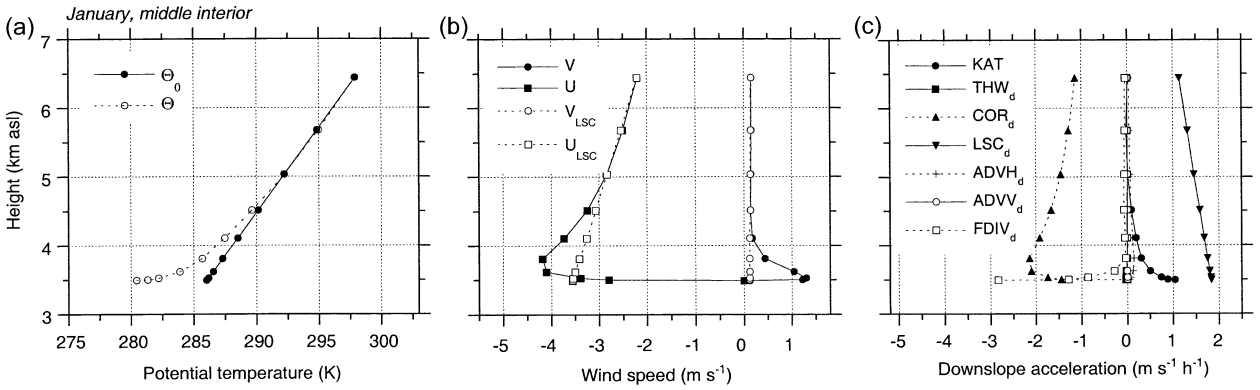

FIG. 5. Average Jan (1980–93) vertical profiles in middle interior bin (3250–3750 m ASL) of (a) potential temperature, (b) down- and cross-slope wind components, and (c) downslope momentum budget. See text for further explanation.

(see also Fig. 4b). The thickening of the ABL toward the coast sets up a significant opposing THW_d that effectively decelerates the katabatic flow over the coastal slopes, especially higher in the ABL. The cold air that is so ''trapped'' over the steep slopes results in large values of KAT (Fig. 8c) and strong easterly winds in a more than 2-km-thick layer (Fig. 8b).

6. Horizontal profiles in the surface layer

Figures 9 (January) and 10 (July) show horizontal profiles of (a) potential temperature, (b) wind components, and (c) downslope momentum budget as a function of distance to the coast (negative values indicate ice sheet bins). Data are taken from the lowest model layer, which is situated about 7 m above the ground. From now on this will be referred to as the surface layer (SL).

a. January

Over the ice sheet, the January temperature perturbation in the SL becomes more negative from the coast to 600 km inland, but then remains constant or slowly decreases (Fig. 9a). This decrease reflects the stronger insolation further south. The 10-K increase in Θ_0 from the coast to the interior of the ice sheet is composed of the surface elevation increase in a stably stratified atmosphere (+16 K for a background lapse rate of 5 K km^{-1}) that is partly offset by a colder free atmosphere in the interior (−6 K). The absolute wind speed increases gradually toward the coast (Fig. 9b), reaching a maximum of 7 m s^{-1} at 1500 m asl. LSC_d dominates the momentum balance (Fig. 9c), and U closely follows U_{LSC} (Fig. 9b), except near the coast where KAT becomes equally important. Over the ice sheet, THW_d contributes positively to the downslope acceleration in the distance interval −100 to −800 km, indicative of a decreasing integrated ABL temperature perturbation toward the coast. This changes in a slight opposing force over the shelves (Fig. 9c), showing that the piling up of cold air, albeit weak, is also present in summer.

b. July

In contrast to January, Θ_0 in the SL is fairly constant in the interior ice sheet in July (Fig. 10a); the increase in Θ_0 one would expect from the increasing elevation in a statically stable atmosphere is offset by the effect of a colder free atmosphere toward the interior. Over

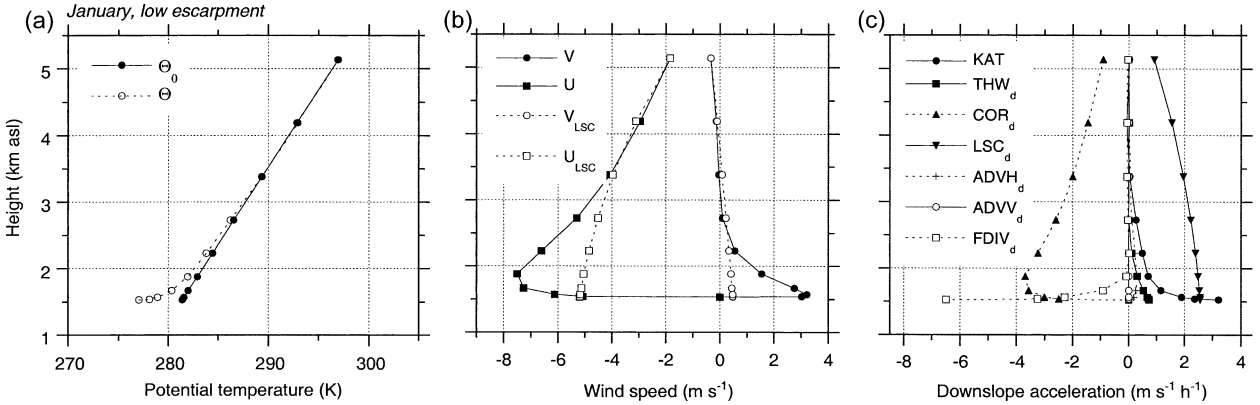

FIG. 6. As in Fig. 5, but for low escarpment bin (1250–1750 m ASL).

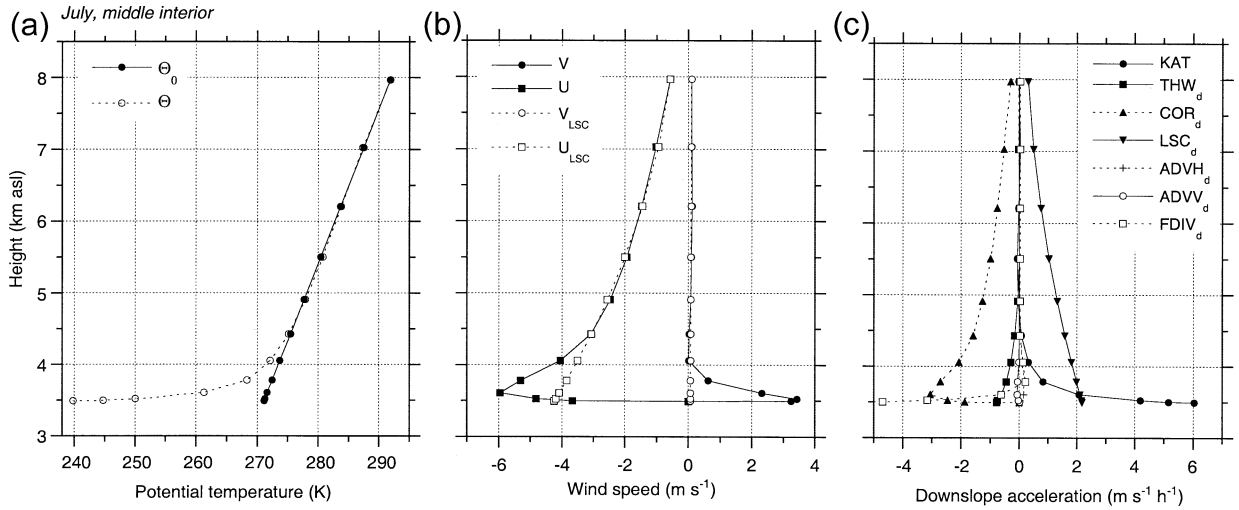

FIG. 7. Average Jul (1980–93) vertical profiles in middle interior bin (3250–3750 m ASL) of (a) potential temperature, (b) down- and cross-slope wind components, and (c) downslope momentum budget. See text for further explanation.

the ocean, Θ_0 in the SL decreases steadily toward Antarctica and reaches a minimum over the ice shelves, after which it increases quickly in response to enhanced subsidence in the ABL over the escarpment of the ice sheet in the area of strong katabatic winds. Here, Θ decreases much faster toward Antarctica than Θ_0, indicating the presence of a substantial temperature deficit over the sea ice. A local minimum in Θ is reached over the ice shelves, after which it strongly increases over the slopes of the ice sheet in response to enhanced mixing by katabatic winds; this maximum in near-surface Θ agrees with observations (van den Broeke et al. 1999). The temperature perturbation Δ_Θ ranges from -15 to -25 K; it slightly increases in the highest ice sheet elevation bin, probably in response to enhanced subsidence over the major ice domes (see section 6d).

KAT dominates the July SL momentum budget over the ice sheet (Fig. 10c) to such a degree that wind speeds in the SL in the bins near the coast exceed the large-scale winds, in spite of the proximity of the surface and the associated drag (Fig. 10b). Over the coastal ice sheet, THW_d becomes as important a decelerating force in the SL as surface drag. Horizontal and vertical advection are once more small. Over the adjacent ocean, the bulge of cold air will initially drain northward and then turn into easterlies by the Coriolis effect. For the first 300 km over the ocean, THW and LSC thus work together to force easterly winds in the surface layer. From 300–500 km, LSC is of the opposite sign but does not exceed THW. At greater distances, LSC exceeds THW so that westerlies are found in the surface layer. However, even at 900-km distance THW compensates about 25% of

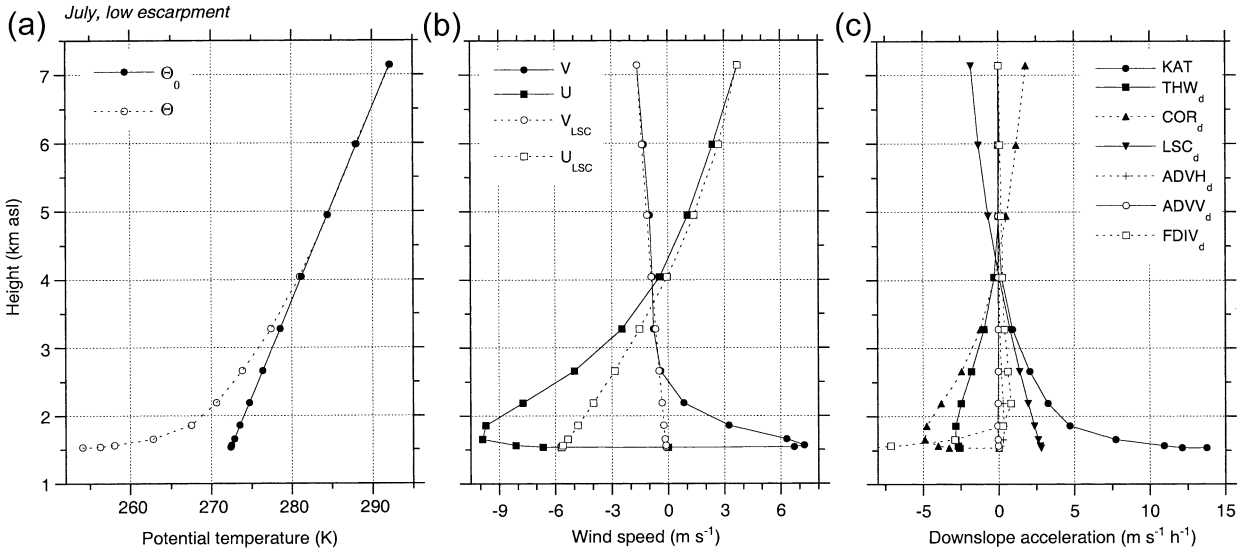

FIG. 8. As Fig. 7, but for low escarpment bin (1250–1750 m ASL).

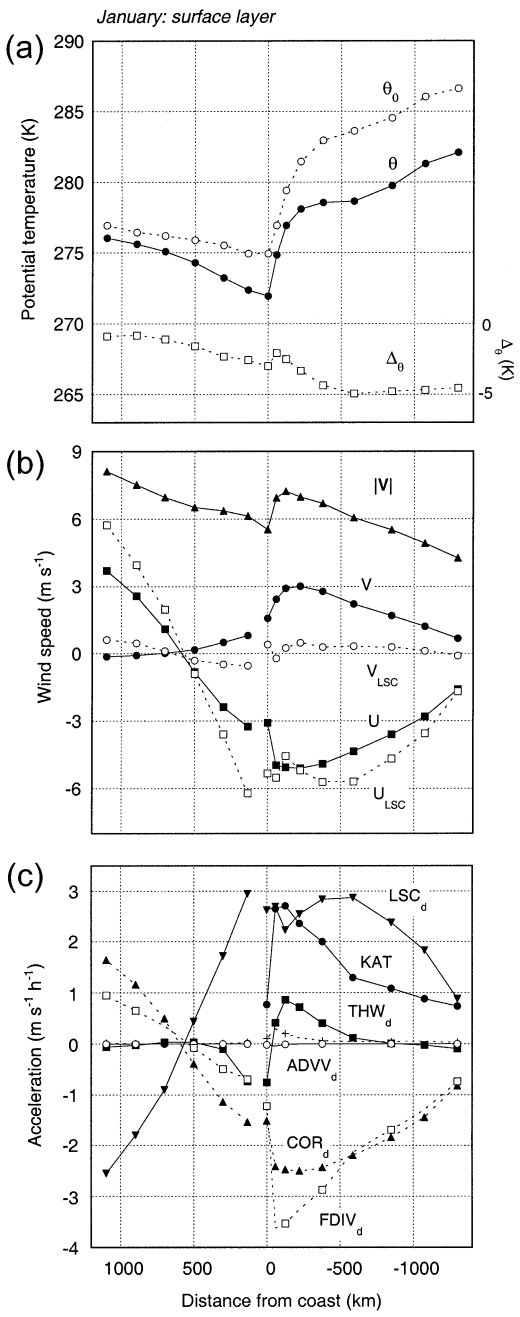

FIG. 9. Average Jan (1980–93) horizontal profile in the surface layer (lowest model layer, 6–7 m above ground level) of (a) potential temperature (perturbation), (b) down- and cross-slope wind components, and (c) downslope momentum budget. See text for further explanation.

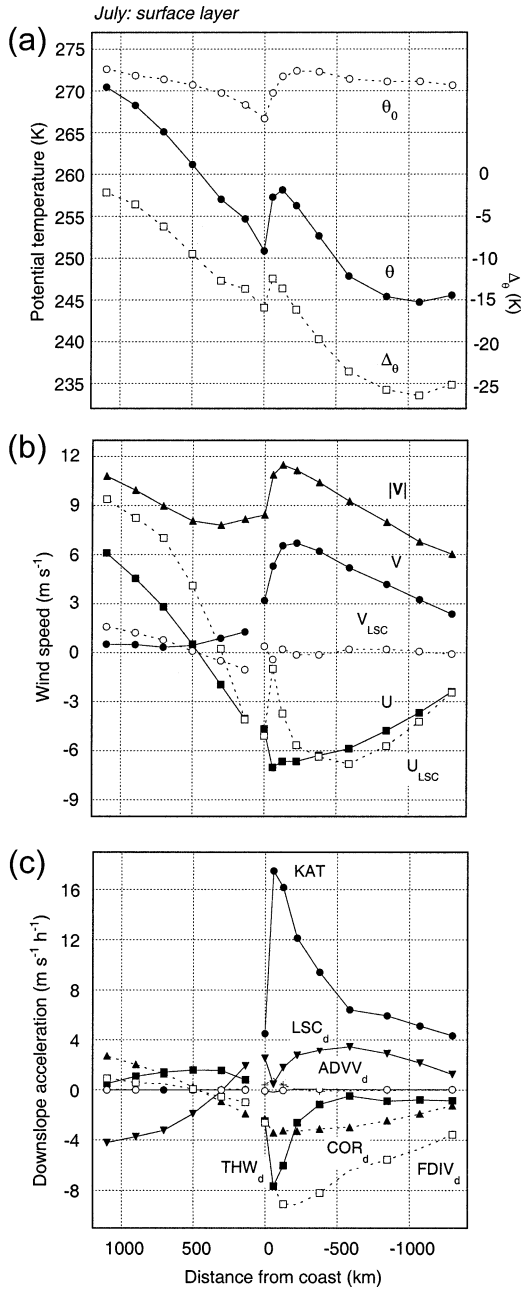

FIG. 10. As in Fig. 9, but for average Jul conditions (1980–93).

LSC so that westerlies in the SL are considerably weaker than would be the case in a horizontally homogeneous ABL.

c. Directional constancy

Figure 11 shows horizontal profiles of wind directional constancy DC [see Eq. (1)]. In July, the dominance of KAT over the more variable LSC_d leads to higher DC in the interior (Fig. 11). Because LSC_d works in the same direction as KAT, a steady wind direction is retained in January and DC remains high, especially near the coast where large-scale easterlies are stronger in summer than in winter. Over the ocean, the southward shift of the CPT in winter is clearly visible. This happens in response to increased meridional temperature gradients, which enhances depression activity. Note that the CPT is even closer to the continent in the equinoctial months (not shown) as a result of the semiannual os-

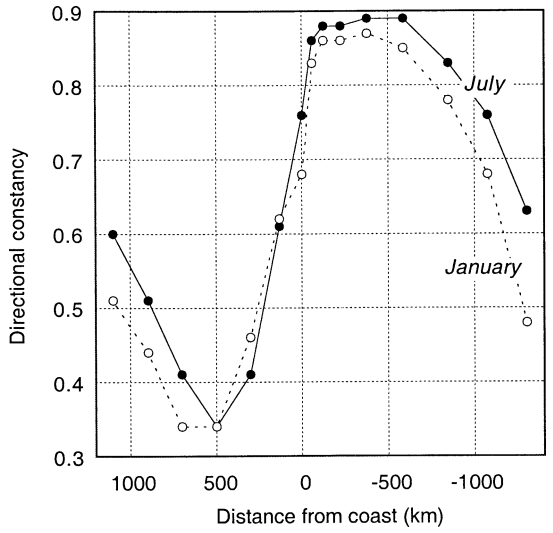

FIG. 11. Average (1980–93) horizontal profile in the surface layer of directional constancy for Jan (dashed line) and Jul (solid line).

cillation (van Loon 1967). The annual cycle of the ABL momentum budget will be discussed in a forthcoming paper.

d. Vertical velocity

The downslope component of East Antarctic katabatic winds is small and confined to a shallow layer under the wind speed maximum, so that only modest mass flux divergence is possible. Figure 12 shows the vertical distribution of vertical velocity W in the ABL for (a) January and (b) July, for selected elevation bins. Sinking motion is found in the interior, roughly twice as strong in July as in January, reflecting the acceleration of the katabatic winds toward the coast. The ''piling up'' of cold air over the sea ice and ice shelves and the associated deceleration of the ABL flow is apparent from rising motion in the bins near the coast. Average vertical velocities do not exceed 0.5 cm s^{-1}, much less than previous estimates (Kottmeier 1988). Note that mass flux divergence as well as horizontal momentum advection could become much more important *locally* when model resolution is increased (Gallée and Schayes 1992; Kikuchi and Ageta 1989).

Relatively large downward motions are found in bin 1 (>3750 m ASL) in July, in spite of the modest horizontal ABL velocities. This elevation interval includes only the main ice domes of East Antarctica. From these domes, cold air flows away in a radial fashion, causing near-continuous sinking motion in the ABL (Businger and Rao 1965). This sinking motion represents a heating source in a stably stratified atmosphere, which also explains the slight increase of surface layer potential temperatures in winter compared to the lower elevation bins (Fig. 10). The heat budget of the Antarctic ABL will be discussed in more detail in a forthcoming paper.

7. Summary and future work

We quantified the terms in the momentum budget of the East Antarctic atmospheric boundary layer (ABL), for January and July, averaged in nine surface elevation bins over the ice sheet and six distance bins over the oceans. It is found that the topography and physical characteristics of the East Antarctic ice sheet determine the pressure, temperature and wind fields both in the

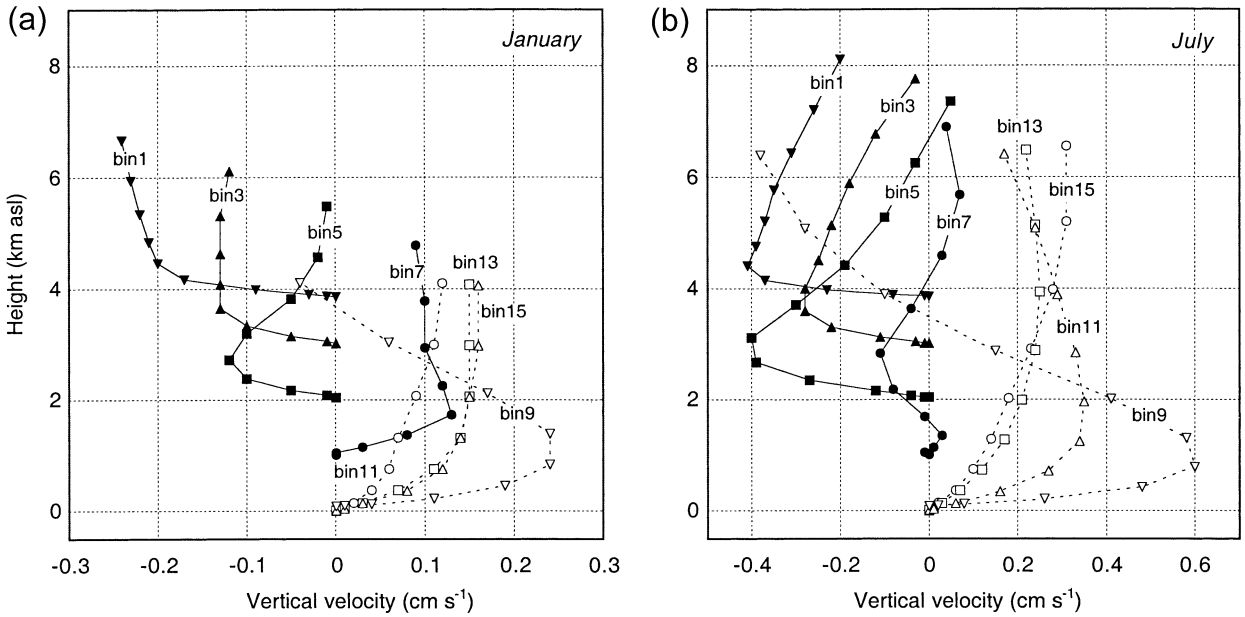

FIG. 12. Average (1980–93) vertical velocity (cm s^{-1}) in selected bins for (a) Jan and (b) Jul.

ABL and in the free troposphere. As a result, pressure gradient forces in the cross-slope direction are small. Directionally constant easterly large-scale winds drive the motion in the ice sheet ABL in January, when surface cooling is weak. In July, a pronounced but shallow katabatic jet develops over the interior, but in the coastal region, the katabatic force dominates in the lowest 3 km. The piling up of cold air over the adjacent sea ice and ice shelves sets up a considerable opposing force. Intraseasonal changes of the large-scale easterlies over the ice sheet can be explained in terms of the strength of the polar vortex, background baroclinicity and the topography of the East Antarctic ice sheet.

Subsidence is found in the ABL over the interior ice sheet and rising motion in the coastal zone, reflecting the acceleration and deceleration of katabatic winds. Mean vertical velocities are small, typically <0.5 cm s^{-1}, because the downslope component of the ABL wind is confined to a shallow layer below the wind speed maximum, which limits the potential downslope mass flux divergence. However, these results should be viewed in light of the dependence of model resolution: mass flux divergence and horizontal advection effects will become more important at higher model resolution.

In the near future we plan to use RACMO/ANT1 model output to explore in more detail the regional and temporal variations of the momentum, heat and moisture budget of the Antarctic ABL. Special attention will be given to the climate of the two large ice shelves, where the katabatic force is still appreciable (Kottmeier 1986; King 1993) and the coupling of the ABL climate to slow oscillations such as the semiannual oscillation (van den Broeke 2000a,b). In the near future, it is planned to start a run with an improved model version (RACMO/ANT2), at higher resolution in the horizontal and vertical and for the full period of the 1958–98 ECMWF reanalysis (ERA-40).

Acknowledgments. This work has benefited from the comments made by three anonymous reviewers. This is EPICA publication no. 45. This work is a contribution to the European Project for Ice Coring in Antarctica (EPICA), a joint ESF (European Science Foundation)/EC scientific programme, funded by the European Commission under the Environment and Climate Programme (1994–1998) Contract ENV4-CT95-0074 and by national contributions from Belgium, Denmark, France, Germany, Italy, the Netherlands, Norway, Sweden, Switzerland, and the United Kingdom.

REFERENCES

Allison, I., G. Wendler, and U. Radok, 1993: Climatology of the East Antarctic ice sheet (100°E to 140°E) derived from automatic weather stations. *J. Geophys. Res.,* **98** (D5), 8815–8823.

Bromwich, D. H., and Y. Du, 1994: Numerical simulation of winter katabatic winds from West Antarctica crossing Siple Coast and the Ross Ice Shelf. *Mon. Wea. Rev.,* **122,** 1417–1435.

——, and Z. Liu, 1996: An observational study of the katabatic wind confluence zone near Siple Coast, West Antarctica. *Mon. Wea. Rev.,* **124,** 462–477.

Businger, J. A., and K. R. Rao, 1965: The formation of drainage wind on a snow dome. *J. Glaciol.,* **7,** 833–841.

Connolley, W. M., 1996: The Antarctic temperature inversion. *Int. J. Climatol.,* **16,** 1333–1342.

Denby, B., 1999: Second-order modelling of turbulence in katabatic flows. *Bound.-Layer Meteor.,* **92,** 67–100.

Gallée, H., and G. Schayes, 1992: Dynamical aspects of katabatic winds evolution in the Antarctic coastal zone. *Bound.-Layer Meteor.,* **59,** 141–161.

——, P. Pettré, and G. Schayes, 1996: Sudden cessation of katabatic winds in Adélie Land, Antarctica. *J. Appl. Meteor.,* **35,** 1129–1141.

Genthon, C., and A. Braun, 1995: ECMWF analysis and predictions of the surface climate of Greenland and Antarctica. *J. Climate,* **8,** 2324–2332.

Hines, K. M., D. H. Bromwich, and T. R. Parish, 1995: A mesoscale modeling study of the atmospheric circulation of high southern latitudes. *Mon. Wea. Rev.,* **123,** 1146–1165.

Kikuchi, T., and Y. Ageta, 1989: A preliminary estimate of inertia effects in a bulk model of katabatic wind. *Proc. NIPR Symp. Polar Meteor. Glaciol.,* **2,** 61–69.

King, J. C., 1993: Control of near-surface winds over an Antarctic ice shelf. *J. Geophys. Res.,* **98** (D7), 12 949–12 953.

——, 1996: Longwave atmospheric radiation over Antarctica. *Antarct. Sci.,* **8,** 105–109.

Kodama, Y., G. Wendler, and N. Ishikawa, 1989: The diurnal variation of the boundary layer in summer in Adélie Land, Eastern Antarctica. *J. Appl. Meteor.,* **28,** 16–24.

Kottmeier, C., 1986: Shallow gravity flows over the Ekström Ice Shelf. *Bound.-Layer Meteor.,* **35,** 1–20.

——, 1988: Atmosphärische Strömungsvorgänge am Rande der Antarktis. *Berichte des Institutes für Meteorologie und Klimatologie der Universität Hannover,* Vol. 33, Ph.D. thesis, University of Hanover, 153 pp.

Mahrt, L., 1982: Momentum balance of gravity flow. *J. Atmos. Sci.,* **39,** 2701–2711.

Parish, T. R., and D. H. Bromwich, 1987: The surface windfield over the Antarctic ice sheets. *Nature,* **328,** 51–54.

——, and K. T. Waight, 1987: The forcing of Antarctic katabatic winds. *Mon. Wea. Rev.,* **115,** 2214–2226.

——, and J. J. Cassano, 2001: Forcing of the wintertime Antarctic boundary layer winds from the NCEP–NCAR global reanalysis. *J. Appl. Meteor.,* **40,** 810–821.

Pettré, P., and J. C. André, 1991: Surface pressure change through Loewe's phenomena and katabatic flow jumps: Study of two cases in Adélie Land, Antarctica. *J. Atmos. Sci.,* **48,** 557–571.

Schwerdtfeger, W., 1970: The climate of the Antarctic. *World Survey of Climatology,* H. E. Landsberg, Ed., Vol. 14, Elsevier, 253–355.

Streten, N. A., 1990: A review of the climate of Mawson—A representative strong wind site in East Antarctica. *Antarct. Sci.,* **2,** 79–89.

van den Broeke, M. R., 1997: Spatial and temporal variation of sublimation on Antarctica: Results of a high-resolution general circulation model. *J. Geophys. Res.,* **102** (D25), 29 765–29 778.

——, 2000a: On the interpretation of Antarctic temperature time series. *J. Climate,* **13,** 3885–3889.

——, 2000b: The semi-annual oscillation and Antarctic climate. Part 5: Impact on the annual temperature cycle as derived from NCEP re-analysis. *Climate Dyn.,* **16,** 369–377.

——, and R. Bintanja, 1995: Summer time atmospheric circulation in the vicinity of a blue ice area in east Queen Maud Land, Antarctica. *Bound.-Layer Meteor.,* **72,** 411–438.

——, R. S. W. van de Wal, and M. Wild, 1997: Representation of Antarctic katabatic winds in a high-resolution GCM and a note on their climate sensitivity. *J. Climate,* **10,** 3111–3130.

——, J.-G. Winther, E. Isaksson, J. F. Pinglot, L. Karlöf, T. Eiken, and L. Conrads, 1999: Climate variables along a traverse line

in Dronning Maud Land, East Antarctica. *J. Glaciol.*, **45,** 295–302.

van Lipzig, N. P. M., 1999: The surface mass balance of the Antarctic ice sheet: A study with a regional atmospheric model. Ph.D. thesis, Utrecht University, 154 pp. [Available from IMAU, P.O. Box 80005, 3508 TA Utrecht, Netherlands.]

——, E. van Meijgaard, and J. Oerlemans, 1998: Evaluation of a regional atmospheric climate model for January 1993, using in situ measurements from the Antarctic. *Ann. Glaciol.*, **27,** 507–514.

——, ——, and ——, 1999: Evaluation of a regional atmospheric model using measurements of surface heat exchange processes from a site in Antarctica. *Mon. Wea. Rev.*, **127,** 1994–2011.

van Loon, H., 1967: The half-yearly oscillation in the middle and high southern latitudes and the coreless winter. *J. Atmos. Sci.*, **24,** 472–486.

Weller, G., 1969: A meridional wind speed profile in MacRobertson Land, Antarctica. *Pure Appl. Geophys.*, **77,** 193–200.

Wendler, G., J. C. André, P. Pettré, J. Gosink, and T. Parish, 1993: Katabatic winds in Adélie coast. *Antarctic Meteorology and Climatology: Studies Based on Automatic Weather Stations*, D. H. Bromwich and C. R. Stearns, Eds., Antarctic Research Series, Vol. 61, Amer. Geophys. Union, 23–46.